THE JOURNAL OF PHYSICAL CHEMISTRY A
A JOURNAL OF THE AMERICAN CHEMICAL SOCIETY

pubs.acs.org/JPCA Article

Rational Design of Organic Emitters with Inverted Singlet−Triplet Gaps for Enhanced Exciton Management

Sanyam,[†] Priyanshu Sorout,[†] and Anirban Mondal*

Cite This: https://doi.org/10.1021/acs.jpca.4c03443 Read Online

ACCESS | Metrics & More | Article Recommendations | Supporting Information

ABSTRACT: In organic light-emitting diodes (OLEDs), the pursuit of efficient molecular emitters has led to the development of thermally activated delayed fluorescence (TADF) molecules. While TADF compounds have promising properties, they face challenges such as energy gap constraints and uphill exciton transfer. Inverted emitters (INVEST) offer a novel solution with an inverted singlet−triplet energy (ΔE_{ST}) gap, enabling efficient utilization of excitons. This study examines the design and computational analysis of an array of molecules, including 23 INVEST emitters and remaining with positive energy gaps. Within the STEOM-DLPNO−CCSD framework, we explore the role of various molecular fragments in determining ΔE_{ST}. We also assess the importance of dynamic spin-polarization (DSP) obtained via the Pariser−Parr−Pople (PPP) scheme in energy gap determination. Exciting trends emerged from our results, with pentalene-containing compounds consistently manifesting negative ΔE_{ST} values while their naphthalene counterparts exhibited contrasting behavior. Moreover, we observed a negative DSP correlates with inverted singlet−triplet gaps. Overall, this research advances OLED materials through molecular design and computational analysis, offering avenues for optimizing exciton management and enhancing device performance.

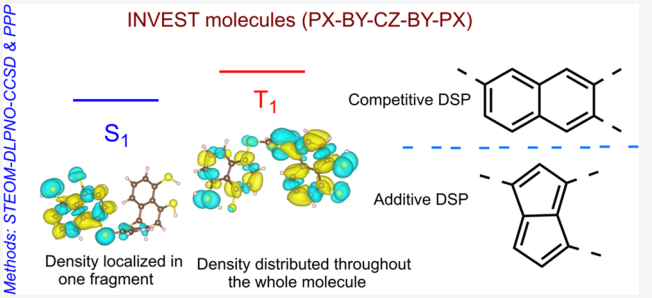

1. INTRODUCTION

Thermally activated delayed fluorescence (TADF) emitters signify a promising cohort of compounds adept at efficiently harnessing excitons from both singlet (S_1) and triplet (T_1) states, thereby achieving internal quantum efficiencies (IQE) and photoluminescence quantum yields (PLQY) approaching perfection.[1−3] However, specific parameters constrain their utilization. Primarily, the energy gap between S_1 and T_1 states must remain below 0.2 eV.[4−6] Even when this condition is met, excitons still necessitate transfer to the S_1 state from T_1 during the uphill transition, thereby delaying the fluorescence process. This delay originates from positioning the T_1 state beneath the S_1 state, governed by Hund's rule of maximum multiplicity,[7,8] wherein the T_1 state is energetically favored. Consequently, thermal activation of excitons in the T_1 state becomes crucial, facilitating their migration to the S_1 state and subsequent emission. An alternative category of compounds, known as inverted singlet−triplet (INVEST) molecules, has been explored to circumvent this inherent challenge.[9−11] Unlike TADFs, these molecules do not adhere to Hund's rule,[12−14] setting the T_1 state above that of S_1 state. Consequently, the activation of electrons from the T_1 state becomes unnecessary, and the transition from T_1 to S_1 becomes a downhill process conducive to emission. As a result of this downhill process, the time delay for fluorescence due to the reverse intersystem crossing (RISC) process also diminishes.

In 1980, Leupin and Wirz discovered that certain compounds, such as cyclazine and azaphenalene, could achieve negative singlet−triplet energy gaps.[15] Their experiments, based on energy transfer, revealed triplet state lifetimes on the order of 100 ns. Similarly, Domcke et al. conducted a study with a heptazine derivative using time-resolved photoluminescence spectroscopy. Surprisingly, they found no evidence of delayed fluorescence and detected no presence of the triplet state.[16−19] This finding was further corroborated by researchers at RIKEN, who also investigated a heptazine derivative.[20] Their temperature-dependent transient photoluminescence spectroscopy demonstrated that the rate of reverse intersystem crossing exceeded that of intersystem crossing (ISC). An additional significant observation was made regarding the negative singlet−triplet gap, attributing it to dynamic spin polarization (DSP),[7,8,12,13] which favors the stabilization of the singlet state over the triplet state. Several fused aromatic hydrocarbons with $(4n + 2)\pi$ electrons and antiaromatic compounds with $4n\pi$ electrons were reported and

Received: May 24, 2024
Revised: July 31, 2024
Accepted: August 12, 2024

compared in relevant studies.[12,13] Recently, Aizawa et al. demonstrated the role of DSP in stabilizing the S_1 state.[21]

Computational research plays a pivotal role in exploring the potential of INVEST molecules in organic electronics. Among the compounds investigated by the computational chemistry community, boron- and/or nitrogen-doped phenalene-type structures predominate, with exceptions such as azulene and pentalene among polyaromatic hydrocarbons.[14,20,22−25] The inversion of the triplet state can be attributed to minimal exchange and limited spatial overlap between the highest occupied molecular orbital (HOMO) and lowest unoccupied molecular orbital (LUMO), aiming to maintain a minimal energy gap (ΔE_{ST}). Additionally, it has been suggested that the S_1 wave function should exhibit a greater double excitation character than T_1.[24,26,27] However, achieving a balance between HOMO−LUMO overlap and oscillator strength remains a significant challenge. Pollice et al. conducted extensive computational investigations on phenalene and azaphenalene, exploring various molecular configurations by manipulating the number of rings and nitrogen atoms.[14] Their efforts yielded appreciable oscillator strength values and high fluorescence rates, reaching magnitudes of 10^7 s^{-1}.[14] In a related study, Corminboeuf et al. elucidated the role of symmetry in adjusting ΔE_{ST}, emphasizing the importance of delocalization and well-separated HOMO−LUMO in INVEST molecule design. They achieved an oscillator strength value of the order 0.01 for most of the compounds.[28,29] Furthermore, Omar et al. undertook an intriguing effort, exploring a chemical space of 15,000 compounds via high throughput screening. Their findings identified seven compounds with a negative singlet−triplet gap.[30] Despite these efforts, the key questions arise: How can computational methods be further refined to enhance the prediction accuracy of INVEST molecule properties?

Building upon these insights, our study delves into exploring the diverse photophysical parameters of a set of potential INVEST compounds. We designed 32 distinct molecules, integrating core fragments, bridging atoms, and peripheral moieties. Benzene, thiophene, pyrrole, and furan served as the core components, while oxygen and sulfur were chosen as bridging atoms and pentalene and naphthalene as peripheral moieties. By selecting separate fragments for the core, bridging atom, and peripheral units, we aimed to exploit the separated HOMO−LUMO nature. Utilizing the transformed equation of motion method augmented with the domain-based on local pair natural orbitals (DLPNO) approach (STEOM-DLPNO−CCSD), we calculated the energy gap (ΔE_{ST}) values. As a wave function-based technique and a computationally efficient alternative to Coupled Cluster Singles and Doubles (CCSD), this method accurately accounts for double excitations and dynamic spin polarization, ensuring precise ΔE_{ST} predictions.[22,23,31,32] Moreover, leveraging STEOM-DLPNO−CCSD, as in our prior works on TADF emitters, strengthens the reliability of our findings.[33,34] Our investigation extends beyond ΔE_{ST} estimation to characterize excitons. Additionally, we computed exchange integrals, HOMO−LUMO overlaps, and dynamic spin polarization using the Pariser−Parr−Pople (PPP) method, which corroborates our results.[35−40] Remarkably, our investigations yielded high spin−orbit coupling values ($H_{SO}^{S_1T_1}$), indicative of robust reverse intersystem crossing (RISC) rates on the order of 10^7 s^{-1}. Complementing our quantitative analyses, qualitative insights were gleaned through frontier molecular orbital plots and density difference diagrams. Notably, our results delineate a trend where compounds featuring pentalene units as peripheral moieties exhibit an inverted gap, while those incorporating naphthalene units manifest a positive gap. This strategic design approach, underscored by our findings, holds substantial promise for advancing efficient OLEDs.

2. METHODS

2.1. Quantum Mechanical Calculations. We deployed a comprehensive computational approach to investigate the designed molecules. The ground-state geometry (S_0) optimization of all 32 molecules was conducted utilizing the B3LYP/6-31+G(d,p) level of theory as implemented in Gaussian 09[41] program. The B3LYP method was selected due to its established reliability in predicting ground-state structural and electronic properties adequately.[42] Subsequently, the ground-state density functional theory (DFT)-optimized geometries were exploited to compute vertical excitation energies of S_1 and T_1 states and the related ΔE_{ST} values. Such protocol was employed primarily to control the computational overhead and was already shown to reproduce the experimental data, as reported by Brédas and co-workers[43] and our earlier benchmark study.[34] The excited states were characterized utilizing the STEOM-DLPNO−CCSD method using `TIGHTSCF` and `TIGHTPNO` keywords and the def2-SVP basis sets implemented in the ORCA program, v.5.0.[44] Due to its ability to adequately account for the higher-order excitations (singles and doubles), the STEOM-DLPNO−CCSD method delivers a precise treatment for the excited-state characteristics of diverse molecules, including TADF-based compounds.[23,33,34] The def2-SVP basis set was employed primarily to reduce the overall computational cost. We have tested the convergence of the cutoff values used for the STEOM-DLPNO−CCSD calculation. The converged cutoff values used were `othresh` = 0.005, `vthresh` = 0.005, and `TCutPNOSingles` = 1×10^{11}. Additionally, we tested the `TCutPNOSingles` = 1×10^{12}, keeping all other parameters the same. We observed no changes in the final energy gaps. The vertical energies and spin−orbit couplings corresponding to 3 excited states (singlets and triplets each) were calculated. The conductor-like polarizable continuum solvent model (CPCM)[45] with toluene (ϵ = 2.4) as the solvent was used to account for the solvent effect. Further, the characterization of excitonic properties, such as the overlap index (S_+) and the distance between the negative and positive barycenters (D_{CT}) of the donor and acceptor moieties, was conducted utilizing Multiwfn[46] software. Given the significant influence of the dynamical spin polarization factor on the inversion of ΔE_{ST}, the Pariser−Parr−Pople[35] model was employed to ascertain DSP values, as well as HOMO−LUMO overlap and exchange integrals. This comprehensive approach ensures a thorough analysis of excitonic behavior, essential for advancing our understanding of INVEST molecules. All the optimized geometries of the investigated molecules are provided in a separate compressed file as additional Supporting Information (SI). The estimated S_1 and T_1 energies are tabulated in Table S1 of the SI. Also, a sample input file is provided in Section S1 of the SI.

2.2. Materials Design Strategy. The careful selection of materials and design strategy is instrumental in fine-tuning the photophysical properties of emitter compounds. In this study, we implemented a systematic workflow to conceive and evaluate 32 potential INVEST molecules, detailed in Figure 1.

https://doi.org/10.1021/acs.jpca.4c03443
J. Phys. Chem. A XXXX, XXX, XXX−XXX

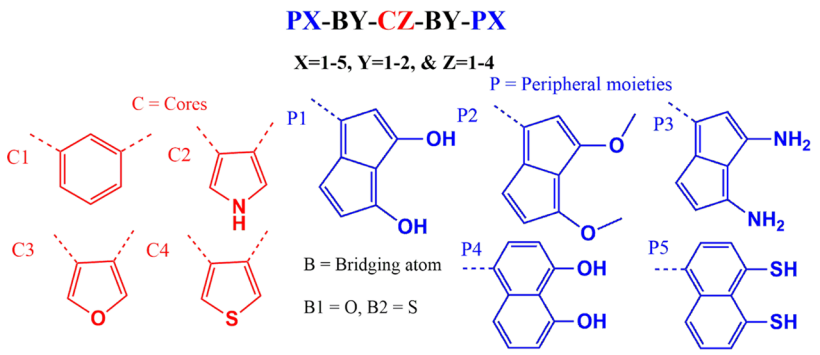

Figure 1. Chemical structures of the building blocks utilized to design potential INVEST molecules in this study. *X* and *Y* values are the same on both sides. The complete molecular structures are shown in Figure S1 of the SI.

Each molecule comprises three integral elements: core units, bridging atoms, and peripheral units. The core units, including benzene, pyrrole, furan, and thiophene, were carefully chosen for their structural properties. Pentalene and naphthalene were selected as peripheral units, with pentalene particularly favored for its high symmetry (D_{2h}), as elucidated in Corminboeuf et al.'s recent research, which highlights its suitability for use as inverted gap emitters.[28,29] This study also noted that transitioning from less symmetric (C_{2h}) to more symmetric (D_{2h}) hydrocarbons enhances the propensity for inverted gap formation. Also, it was shown in the literature that the molecules with triangular shapes possess a negative singlet−triplet gap.[47] However, symmetry is insufficient to cause the singlet−triplet gap to be inverted, as elaborated in ref 48. The other related study explains that the planar geometry of the molecules leads to severe aggregation-caused quenching (ACQ), which is unsuitable for external quantum efficiency (EQE).[49] So, to make the molecule nonplanar and to separate the HOMO and LUMO, we have adopted such kind of designing strategy. To facilitate comparative analysis, we included pentalene, with a $4n\pi$ electron system, and naphthalene, with a $(4n + 2)\pi$ electron system. Bridging was accomplished using bivalent atoms, specifically oxygen and sulfur, with sulfur chosen for its high atomic number and propensity for spin−orbit coupling effects. Maintaining adequate overlap required positioning the core ring centrally, with bridging atoms substituting meta positions for benzene and ortho positions for pyrrole, furan, and thiophene. Substitutions such as $-NH_2$, $-OH$, $-SH$, and $-OCH_3$ were introduced on the peripheral moieties to examine electronegativity effects and the electron donating/accepting tendencies of the peripheral units.

The nomenclature convention used for the designed molecules is the following: the general molecular architecture comprises three distinct units, i.e., C, B, and P. In this context, C denotes the core moiety, with four distinct cores identified as C1, C2, C3, and C4, as depicted in Figure 1. The bridging atoms are denoted by B, with bivalent oxygen (O) and sulfur (S) designated as B1 and B2, respectively. Lastly, the peripheral units labeled as P, ranging from P1 to P5, are affixed to the bridging atoms on both ends. The core component is centrally positioned, with bridging atoms on either side via the depicted dotted line in Figure 1. Then, the peripheral units are attached to the bridging atoms on both sides. Noteworthy is the omission of bridging atoms and peripheral units on the left side in Tables 1 and 2, a measure taken for shorter nomenclature and avoid larger names.

Table 1. STEOM-DLPNO−CCSD Predicted Quantities of the Designed Molecules: Energy Gap between S_1 and T_1 (ΔE_{ST}, eV), Oscillator Strength (f) Corresponding to S_1 to S_0 Transition, and HOMO−LUMO Energy Gap ($\Delta E_{HOMO\text{-}LUMO}$, eV)

compounds	ΔE_{ST}	f	$\Delta E_{HOMO-LUMO}$
C1−B1−P2	−0.164	0.001	8.24
C1−B1−P3	−0.189	0.006	8.03
C1−B1−P1	−0.515	0.005	8.12
C2−B1−P1	−0.141	0.003	8.22
C2−B1−P2	−0.374	0.001	8.00
C3−B1−P2	−0.351	0.001	8.15
C4−B1−P2	−0.338	0.001	8.18
C2−B1−P3	−0.126	0.010	8.04
C3−B1−P3	−0.229	0.010	8.03
C4−B1−P3	−0.083	0.010	7.98
C1−B2−P1	−0.150	0.012	8.10
C2−B2−P1	−0.163	0.013	8.09
C3−B1−P1	−0.155	0.003	8.32
C2−B2−P2	−0.187	0.008	7.86
C2−B2−P3	−0.654	0.006	7.77
C3−B2−P3	−0.084	0.010	7.67
C4−B2−P3	0.028	0.000	7.62
C3−B2−P2	−0.194	0.010	7.73
C4−B2−P2	−0.458	0.011	7.49
C1−B2−P2	−0.169	0.009	7.86
C4−B2−P1	−0.115	0.005	8.07
C3−B2−P1	−0.103	0.004	7.93
C4−B1−P1	−0.150	0.003	8.28
C1−B2−P3	−0.250	0.006	7.69
C2−B2−P5	1.538	0.231	9.54
C2−B1−P4	1.246	0.096	9.80
C2−B1−P5	1.544	0.049	9.39
C2−B2−P4	1.435	0.019	9.02
C1−B1−P4	1.370	0.078	9.85
C1−B2−P4	1.692	0.035	9.72
C1−B1−P5	1.486	0.039	9.32
C1−B2−P5	1.450	0.000	9.26

3. RESULTS AND DISCUSSION

3.1. Singlet−Triplet Energy Gap: ΔE_{ST}. Our investigation delves into a comprehensive analysis of photophysical parameters for 32 compounds. Remarkably, 23 of these compounds exhibit negative singlet−triplet (ΔE_{ST}) gaps. We validated the choice of basis set and its impact on the computed ΔE_{ST} values by performing similar calculations using the def2-TZVP(-f) basis set for two representative molecules,

https://doi.org/10.1021/acs.jpca.4c03443
J. Phys. Chem. A XXXX, XXX, XXX−XXX

Table 2. Computed Electronic Properties Using the Pariser−Parr−Pople (PPP) Method of Designed Molecules: Exchange Integral between HOMO and LUMO (K in eV), HOMO−LUMO Overlap ($\Phi_{overlap}$), Dynamic Spin-Polarization (DSP in eV)[a]

compounds	K	$\phi_{overlap}$	DSP	$S_{\pm}$	D_{CT}
C1−B1−P2	9.55×10^{-07}	0.008	−0.000001	0.883	1.237
C1−B1−P3	6.90×10^{-03}	0.414	−0.011896	0.950	0.299
C1−B1−P1	2.87×10^{-03}	0.306	−0.014422	0.635	2.411
C2−B1−P1	7.85×10^{-03}	0.605	−0.009532	0.954	0.094
C2−B1−P2	2.71×10^{-06}	0.011	−0.000007	0.983	0.252
C3−B1−P2	5.54×10^{-03}	0.469	−0.011596	0.619	1.459
C4−B1−P2	5.27×10^{-03}	0.453	−0.011837	0.930	0.295
C2−B1−P3	9.09×10^{-07}	0.006	−0.000001	0.956	0.243
C3−B1−P3	6.62×10^{-03}	0.397	−0.012085	0.612	1.259
C4−B1−P3	3.09×10^{-06}	0.012	−0.000003	0.867	0.212
C1−B2−P1	7.72×10^{-03}	0.602	−0.009473	0.509	2.074
C2−B2−P1	7.64×10^{-03}	0.601	−0.009565	0.556	1.708
C3−B1−P1	8.03×10^{-03}	0.608	−0.009381	0.945	0.196
C2−B2−P2	3.24×10^{-05}	0.055	−0.000041	0.956	0.325
C2−B2−P3	6.52×10^{-03}	0.394	−0.011790	0.662	2.337
C3−B2−P3	4.06×10^{-07}	0.005	0.000000	0.954	0.306
C4−B2−P3	6.50×10^{-07}	0.006	0.000000	0.955	0.220
C3−B2−P2	6.95×10^{-03}	0.566	−0.010305	0.804	0.304
C4−B2−P2	3.29×10^{-03}	0.328	−0.013824	0.824	0.275
C1−B2−P2	4.24×10^{-05}	0.048	−0.000055	0.991	0.204
C4−B2−P1	7.80×10^{-03}	0.607	−0.009428	0.572	1.357
C3−B2−P1	7.78×10^{-03}	0.606	−0.009374	0.779	1.237
C4−B1−P1	7.98×10^{-03}	0.603	−0.009459	0.871	1.240
C1−B2−P3	2.86×10^{-04}	0.078	−0.000465	0.997	0.212
C2−B2−P5	6.61×10^{-09}	0.001	0.000000	0.051	7.457
C2−B1−P4	9.51×10^{-04}	0.203	0.000122	0.231	5.413
C2−B1−P5	1.21×10^{-04}	0.064	0.000015	0.216	6.283
C2−B2−P4	3.79×10^{-07}	0.004	0.000000	0.381	4.613
C1−B1−P4	3.07×10^{-04}	0.106	0.000043	0.247	7.674
C1−B2−P4	3.29×10^{-03}	0.344	0.000425	0.707	2.212
C1−B1−P5	9.77×10^{-06}	0.026	0.000001	0.031	9.497
C1−B2−P5	8.20×10^{-04}	0.175	0.000101	0.785	1.805

[a]Exciton characteristics: overlap integral between the positive and negative barycenters ($S_{\pm}$) during the transition S_1 to S_0 and the distance between the positive and negative barycenters (D_{CT} in Å).

C1−B1−P2 and C1−B1−P3, keeping all other parameters the same. We observed that the S_1 and T_1 energies for C1−B1−P2 and C1−B1−P3 were (1.099, 1.226) and (0.969, 1.119), respectively, yielding ΔE_{ST} values −0.127 and −0.150 eV. The final numbers differ marginally (∼0.04 eV) from def2-SVP level values. These calculated parameters, including ΔE_{ST}, oscillator strength (f), and HOMO−LUMO gap, are summarized in Table 1. As evident from Table 1, compounds featuring the pentalene moiety as the peripheral unit consistently demonstrate negative ΔE_{ST} values, except for compound C4−B2−P3. Conversely, compounds with the naphthalene unit as the peripheral component invariably exhibit positive ΔE_{ST}. This diversity in the ΔE_{ST} values across the studied complexes underscores the subtle interplay of molecular architecture and electronic behavior. Of particular interest is the observation that the most negative ΔE_{ST} value, −0.654 eV, is recorded for complex C2−B2−P3, while the least negative value, −0.083 eV, is attributed to compound C4−B1−P3. A complementary study by Corminboeuf et al.[28] reported 155 computationally designed emitters, of which almost 70% (exactly 107 molecules) possessed negative ΔE_{ST} values. These molecules predominantly featured N-doped compounds. Similarly, in a related work,[29] 187 compounds were scrutinized, albeit without N doping. Surprisingly, only eight compounds exhibited negative ΔE_{ST} values, yielding a markedly lower ratio of achieving INVEST compounds compared to the former report. These calculations were conducted utilizing the CC2/aug-cc-PVDZ method. Recently, Pollice et al. performed a high throughput screening of a large set of potential INVEST emitters consisting of 69,201 candidate structures, out of which 1928 (∼3%) exhibited inverted singlet−triplet energy gaps.[50] In comparison to these studies, our investigation involves compounds without N doping. However, the $-NH_2$ group is a substituent in the peripheral units in substituted rather than fused form. Consequently, the overall ratio of achieving INVEST molecules with inverted singlet−triplet gaps approaches nearly 72%, underscoring our methodology's efficacy in precisely tailoring electronic properties. For comparison, the PPP estimated S_1 and T_1 energies and the ΔE_{ST} are summarized in Table S1 of the SI. We observe positive ΔE_{ST} for most molecules except for a few obtained from the PPP model. To validate the impact of the different solvents in computed ΔE_{ST} and whether the inversion of singlet−triplet gaps is intrinsic to a molecule, we performed additional simulations in hexane solvent for two representative cases: C1−B1−P2 and C1−B1−P3. All other computational protocols were kept the same as reported in the Section 2. The ΔE_{ST} values in hexane solvent were −0.162 and −0.198 eV, respectively, whereas the computed ΔE_{ST} in toluene solvent were −0.164 and −0.189 eV. These comparative numbers thus demonstrate conclusively that the observed singlet−triplet inversion in the examined molecules is intrinsic to the system and not due to an external effect from the solvent considered.

3.2. Frontier Molecular Orbitals. The design strategy employed in tuning the ΔE_{ST} values is elucidated through the distinctive separation HOMO and LUMO, yielding minimized exchange interactions: $\Delta E_{ST} = 2K + DSP$; where K represents the exchange integral and DSP is the dynamic spin polarization. Supporting this strategy, the HOMO−LUMO diagram depicted in Figure S2 of the SI illustrates blue lobes denoting the LUMO and yellow lobes representing the HOMO. Notably, the HOMO localizes on the donor atoms (mainly C and H here). At the same time, the LUMO resides on the acceptor atoms (largely the electronegative hetero atoms, e.g., O, S, and N sites). Across most cases, the HOMO (yellow) and LUMO (blue) lobes exhibit distinct separation, a pivotal factor contributing to the tuning of ΔE_{ST} values. As elucidated in previous work, the rationale behind achieving negative ΔE_{ST} values with the pentalene moiety lies in its inherent property of possessing well-separated HOMO−LUMO states.[29,51] Utilizing symmetry constraints under the D_{2h} point group in the excited state further facilitates minimizing ΔE_{ST} values. However, it is noteworthy that this condition alone is insufficient to confer negative ΔE_{ST} values.

Despite the uniform aromatic character of core components like benzene, thiophene, furan, and pyrrole, the minimal disparity in ΔE_{ST} values is discerned. Drawing upon insights from Yang and Heilbronner's Hückel model,[52] which predicts the alleviation of bond localization by electron-donating substituents at positions with significant LUMO coefficients, we strategically employ donor substituents at LUMO positions.[29] However, it is observed that electron-withdrawing

https://doi.org/10.1021/acs.jpca.4c03443
J. Phys. Chem. A XXXX, XXX, XXX−XXX

substituents are less effective in practice. Keeping that in mind, the selection of oxygen (O) and sulfur (S) atoms as bridging atoms endowed with lone pairs of electrons and exhibiting + R (resonance) effects underscores their role as donor groups. Similarly, based upon the same approach, peripheral positions were decorated with donor units such as −OH, $-OCH_3$, $-NH_2$, and −SH, strategically placed at positions with high LUMO coefficients.[53] The principal role in tuning ΔE_{ST} values lies with the peripheral units and the bridging atoms, with no significant role of the core part observed in our case. We have also calculated the HOMO−LUMO gap for the investigated compounds, tabulated in Table 1. Quantitatively, the HOMO−LUMO gap was observed to be lower for the INVEST molecules, a characteristic distinguishing them from compounds exhibiting positive ΔE_{ST} values. Illustrated in Figure 2, the relationship between the ΔE_{ST} values and the HOMO−LUMO gap is depicted. It is evident that the compounds on the plot's left side, denoted by red circles, predominantly possess negative ΔE_{ST} values, except compound C4−B2−P3. Conversely, compounds characterized by high HOMO−LUMO gap values, represented by blue circles on the right side of the plot, typically exhibit positive ΔE_{ST} values. A green dotted line delineates between negative and positive ΔE_{ST} values.

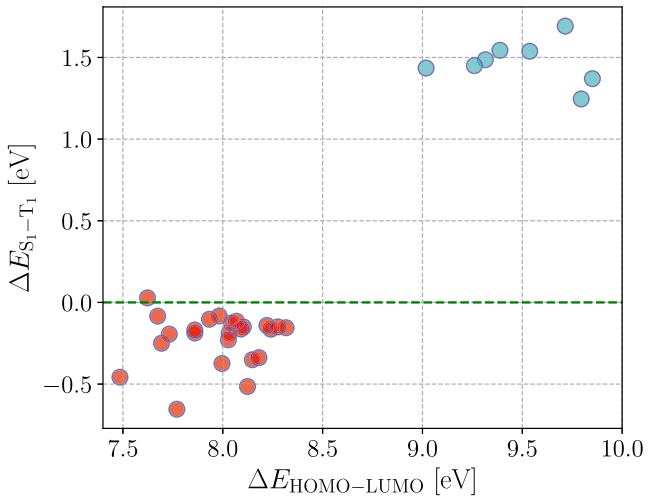

Figure 2. Relation between the ΔE_{ST} and the HOMO−LUMO energy gap of the investigated compounds obtained from STEOM-DLPNO−CCSD calculations. Red and cyan points represent molecules with inverted and positive S_1-T_1 energy gaps. The green dotted line separates the INVEST molecules from those with positive ΔE_{ST} values.

3.3. Oscillator Strength. For a design strategy where the HOMO and LUMO states are well-separated, the oscillator strength tends to be low due to minimal orbital interaction. This presents a significant challenge for such emitters. As elucidated earlier,[28] the Heilbronner strategy currently does not account for oscillator strength. Consequently, like most other inverted gap molecules discussed therein, the compounds predominantly exhibit dark S_1 states owing to the lack of overlap between the HOMO and LUMO, except for a few potential candidates. Furthermore, for these exceptions, the reported oscillator strength was typically of the order of 0.01. In a high-throughput screening of approximately 70,000 compounds, Pollice et al. also categorized molecules as INVEST emitters when their oscillator strength was on the order of 0.01. In our study, among 32 compounds, the highest oscillator strength is reported for compound C2−B2−P5, with an observed value of 0.23. The oscillator strength value in INVEST molecules with a pentalene moiety is lower than that of molecules with a naphthalene moiety. Among the INVEST molecules, the highest oscillator strength is observed for compound C2−B2−P1, with a value of 0.013. The remaining candidates also exhibit appreciable oscillator strengths.

3.4. Dynamic Spin Polarization. It is understood that low exchange integral values and low HOMO−LUMO overlap contribute to minimizing the ΔE_{ST}. However, even after meeting conditions like low HOMO−LUMO overlap and exchange integral, which is often the case for compounds based on thermally activated delayed fluorescence, the ΔE_{ST} value remains positive. Thus, there remains a subsequent challenge that lies in achieving a negative ΔE_{ST} value. An additional stabilization mechanism that aids in achieving a negative ΔE_{ST} value is dynamic spin polarization.[12,13,54−56] In general, a negative DSP value indicates a preference for stabilizing the excited singlet (S_1) state. In contrast, a positive DSP value, often seen, implies an opposing nature, destabilizing the S_1 state and favoring the triplet (T_1) state.[48,57] Therefore, to observe singlet−triplet (ST) inversion, spin polarization is required to lower the energy of the lowest excited singlet state below the energy of the lowest triplet in systems with a small HOMO−LUMO exchange energy.

Electron correlations primarily drive spin polarization and cannot be accurately modeled in single-configuration interaction (CI) approaches. Consequently, time-dependent density functional theory (TD-DFT), arguably the most widely applied quantum-chemical approach to excited states in molecular systems, fails to adequately describe ST inversion, as it typically relies on single excitations and cannot account for the necessary double excitations. Therefore, consideration of at least double excitations is necessary to capture spin polarization, as discussed in work by Bedogni et al.[48] However, their analysis also demonstrated that good indicators for singlet−triplet inversion can already be obtained at the Hartree−Fock (HF) level. Consequently, we estimated the dynamic spin polarization values using the popular Pariser−Parr−Pople (PPP) method.[48] The estimated HOMO−LUMO exchange integral, HOMO−LUMO overlap, and dynamic spin polarization are summarized in Table 2. Figure 3 illustrates the correlation between STEOM-DLPNO−CCSD-computed ΔE_{ST} and dynamic spin polarization obtained from the PPP model for all the investigated systems. As evident, the DSP values are negative for all INVEST compounds except for compound C3−B2−P3. Therefore, it can be seen that if the DSP values are negative, the ΔE_{ST} values are negative, and if the DSP values are positive, the ΔE_{ST} values also become positive except for the compound C3−B2−P3. Such a strong correlation suggests that spin polarization indeed biases the stability of the singlet (S_1) state, resulting in negative ΔE_{ST} values for these molecules. Conversely, there is no additional stabilization of the singlet state for compounds with positive DSP values. Therefore, dynamic spin polarization is a critical descriptor in identifying INVEST emitters.

The HOMO−LUMO overlap is markedly low, as presented in Table 2, indicating an effective separation between the HOMO and LUMO states within this molecular architecture. These values were also obtained using the PPP code.[48] Figure 4 illustrates the relationship between dynamic spin polarization and the exchange integral. Primarily, we are interested in

https://doi.org/10.1021/acs.jpca.4c03443
J. Phys. Chem. A XXXX, XXX, XXX−XXX

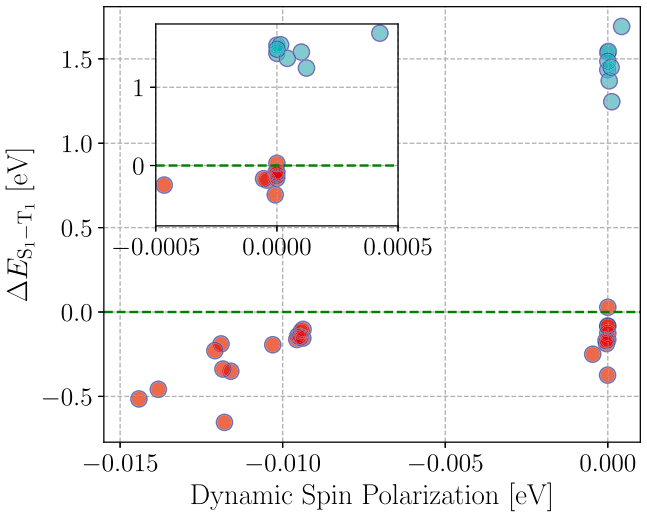

Figure 3. Correlation between STEOM-DLPNO−CCSD-computed ΔE_{ST} and the dynamic spin polarization estimated from the PPP model in the investigated molecules. The green dotted line separates the INVEST molecules from those with positive ΔE_{ST} values. Red and cyan points represent molecules with inverted and positive S_1-T_1 energy gaps.

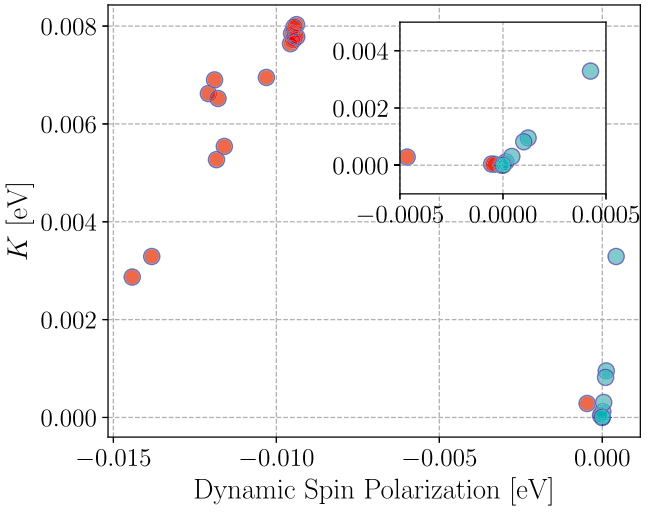

Figure 4. Correlation between the exchange integral and the dynamic spin polarization obtained via the PPP model: red and cyan points represent molecules with inverted and positive S_1-T_1 energy gaps.

finding molecules with low exchange integral accompanied by negative DSP values. Hence, the compounds represented by those points (mainly in red) located toward the left side of Figure 4 are favored when designing INVEST emitters. All molecules possessing an inverted ST gap, except for C3−B2−P3 exhibit negative DSP values, while positive DSP consistently accompanies compounds with positive ΔE_{ST}. Although the exchange values are low for complexes with -P4 and -P5 terminal moieties, another factor such as DSP contribute to maintaining a positive ST gap. All exchange integral values recorded are less than 8.03×10^{-3} eV.

3.5. Exciton Characteristics. In the literature, it has been demonstrated that the exciton character plays a crucial role in the electronic properties, including energy gaps in TADF-based emitters.[34,58] To our knowledge, this aspect has not received significant attention in the case of INVEST emitters. To discern the distinguishing features of INVEST molecules from those with positive ΔE_{ST} values, we studied the exciton parameters. Figure 5 displays the difference density plot for the examined compounds, explicitly concerning the transition from S_0 to S_1. The difference density plots (Δ) were obtained using the following relation: $\Delta = \rho_{ex} - \rho_0$. Here, ρ_{ex} and ρ_0 represent the excited-state (S_1) and ground-state densities, respectively. These plots offer a qualitative understanding of the charge transfer nature inherent in the excited state. As seen in Figure 5, the blue and yellow lobes correspond to the decreased and increased density during the transition. If the blue and yellow lobes are located on alternate atoms within a molecule, it is classified as a locally excited (LE) or short-range charge transfer (SRCT) state. Additionally, in such a state, the pattern may be observed on a specific molecule fragment rather than across the entire molecule. If the yellow and blue lobes are found in different parts of the molecule, it is categorized as a CT state. It is evident from Figure 5 that for compounds with negative ΔE_{ST} values, the yellow and blue lobes are typically situated on alternate atoms, often localized to specific fragments, indicating an LE S_1 state. Conversely, compounds with positive ΔE_{ST} values typically exhibit a CT-type S_1 state, with the observed pattern showing yellow density on one fragment and blue density on another. The density difference plots for the triplet state of the molecules are provided in Figure S3 of the SI. As observed, for the INVEST molecules, the triplet state of the molecules predominantly exhibits a CT-type nature, contrasting with the singlet state, which is essential for the S_1 to T_1 transition.

In addition to Δ, we have evaluated two other important descriptors, $S_\pm$ and D_{CT}, for quantitative assessment of exciton characteristics. $S_\pm$ accounts for the overlap between the positive (increased) and negative (decreased) barycenters (electron density) of the difference density plot. Whereas D_{CT} is defined as the distance between the negative and positive barycenters. An $S_\pm$ value close to 0 is deemed to exhibit a CT state, specifically the long-range charge transfer state (LRCT). Conversely, an $S_\pm$ value close to 1 indicates a locally excited state or the short-range charge transfer (SRCT) state. Similarly, if the D_{CT} parameter is less than 1.6 Å, it implies an LE character; if it exceeds 1.6 Å, it exhibits a CT character.[58] The computed $S_\pm$ and D_{CT} parameters are tabulated in Table 2, yielding direct insights into the behavior of molecules with negative ΔE_{ST} values, indicating the prevalence of locally excited or SRCT nature in their S_1 state. Figure 6 displays the correlation between D_{CT} and S_1-T_1 energy gaps in the studied complexes. As evident, all INVEST molecules are marked with a D_{CT} value around 1.6 Å or less. Contrarily, emitters with positive ΔE_{ST} values possess very high D_{CT} except for C1−B2−P5 and C1−B2−P4. These quantitative estimates further substantiate the qualitative assessment from Figure 5. INVEST molecules demonstrate LE or SRCT-type charge transfer during the S_1 and S_0 transition, whereas the pattern with more long-range character is seen in compounds with positive ST gaps.

3.6. Photophysical Properties. After investigating the ST energy gaps, it becomes imperative to ensure significant spin−orbit coupling between the singlet (S_1) and triplet (T_1) states. High spin−orbit coupling increases intersystem crossing rates between the singlet and triplet states, resulting in higher delayed fluorescence (DF) rates. The spin−orbit coupling between S_1 and T_1 ($H_{SO}^{S_1T_1}$, in cm^{-1}), the energy of the singlet state (in cm^{-1}), ISC rates (in s^{-1}), RISC rates (in s^{-1}), delayed fluorescence (DF) rates (in s^{-1}) and spin−orbit coupling

https://doi.org/10.1021/acs.jpca.4c03443
J. Phys. Chem. A XXXX, XXX, XXX−XXX

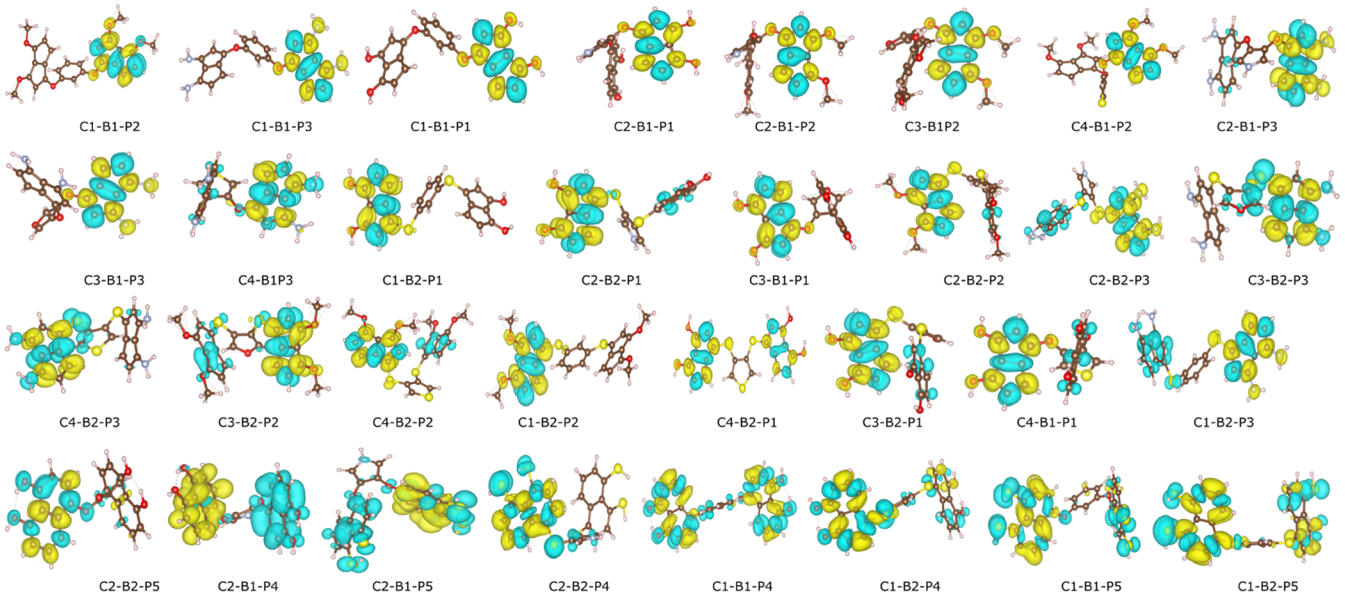

Figure 5. Difference density patterns calculated using STEOM-DLPNO−CCSD method for the emitter molecules for the first singlet excited state (S_1), where blue and yellow lobes represent decreased and increased density, respectively (isovalue = 0.001).

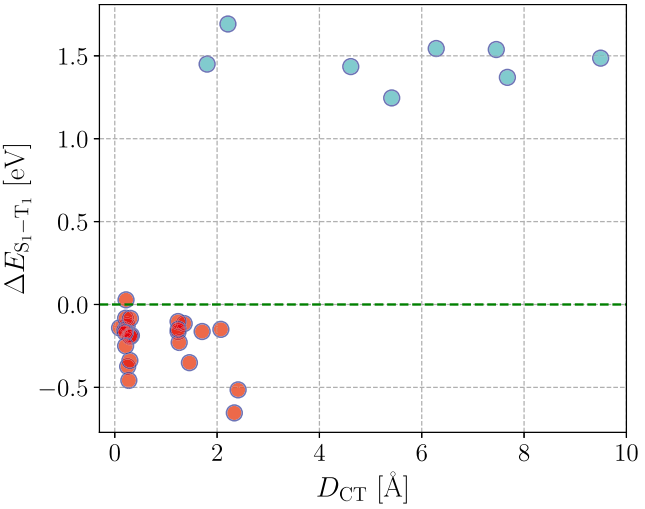

Figure 6. Correlation between the D_{CT} and the ΔE_{ST} in the investigated molecules: red and cyan points represent molecules with inverted and positive S_1-T_1 energy gaps. The green dotted line separates the INVEST molecules from those with positive ΔE_{ST} values.

between S_1 and T_2 ($H_{SO}^{S_1T_2}$ in cm^{-1}) are provided in Table S2 of the SI. The rate constants of RISC (from T_1 to S_1) were estimated within the framework of Fermi's golden rule.[59,60]

$$k_{(R)ISC}^{IF} = \frac{2\pi}{\hbar}|\langle {}^1\psi_I^0|H_{SO}|{}^3\psi_F^0\rangle|^2[FCWD] \quad (1)$$

Here, I and F denote the initial and final excited states, FCWD represents the Franck−Condon weighted density of states, and $\langle {}^1\psi_I^0|H_{SO}|{}^3\psi_F^0\rangle$ defines the spin−orbit coupling. The FCWD term can be described classically in the high-temperature limit.

$$FCWD = \frac{1}{\sqrt{4\pi\lambda k_B T}}\exp\left[-\frac{(\Delta E+\lambda)^2}{4\pi\lambda k_B T}\right] \quad (2)$$

Here, λ is the total reorganization energy, and ΔE is the energy difference between the initial and final states, which is ΔE_{ST} in this context, k_B is the Boltzmann constant, $\hbar$ is the reduced Planck's constant, and T is the room temperature (298 K). The transition rate between the S_1 and T_1 (and vice versa) was determined by three key parameters: the spin−orbit coupling, the energy difference between the two states, ΔE_{ST} (the sign is opposite for RISC and ISC), and reorganization energy λ. Large spin−orbit coupling and small ($\Delta E + \lambda$) are advantageous for these processes. The total reorganization energy is the sum of the inner and outer contributions to reorganization energy. Herein, we have considered 0.2 eV as the total reorganization energy arising from solvation effects.[59,61] The Marcus equation is considered in this study to be suitable for calculating the photophysical rates of these systems, as the reorganization energy of the molecules is high and hence dominates the electron−phonon coupling effects.[62] The formula for the other rates, e.g., fluorescence and delayed fluorescence rates, is provided in SI.

It is evident from Table S2 of the SI that all of the INVEST molecules exhibit nonzero spin−orbit coupling ($H_{SO}^{S_1T_1}$) values except for three: C1−B2−P1, C2−B2−P1, and C4−B2−P2. The observed spin−orbit coupling between S_1 and T_1 states are significant to large in magnitude. Due to high $H_{SO}^{S_1T_1}$, the computed RISC rates are even of the order 10^7 s^{-1} for a few compounds, which is much larger than the traditional MR-TADF compounds,[5,6] rendering them promising candidates for INVEST design. Contrarily, the smaller magnitude of the forward ISC rates is much lower compared to RISC values, which explains the greater utilization of the triplet excitons. For the INVEST emitters with null $H_{SO}^{S_1T_1}$, the utilization of triplet excitons is not feasible as the corresponding RISC rate is also zero. Due to high positive ΔE_{ST}, the computed RISC rates are minimal in the naphthalene-based complexes, leaving those entries in Table S2 of SI. As evident from Table S2 of the SI, for most of the cases, the spin−orbit coupling between the S_1 and T_1 is higher compared to between the S_1 and T_2, which ensures efficient utilization of triplet excitons directly from T_1 to S_1.

It is worth noting that some of the ISC and RISC rate values in Table S2 are zero due to the vanishing spin−orbit coupling

https://doi.org/10.1021/acs.jpca.4c03443
J. Phys. Chem. A XXXX, XXX, XXX−XXX

values between the singlet and triplet states. This suggests that the mechanism may be mediated via vibrational-assisted higher-lying states, which our current methodology does not fully capture. Based on Fermi's golden rule, our approach accounts for the reorganization energy term, reflecting changes in geometry during the transition. However, it does not explain the null spin−orbit coupling values between the singlet and triplet states. Furthermore, it lacks the vibrational correction term to the overall spin−orbit coupling, which arises from specific vibrational modes. Including these corrections could alter the ISC and RISC rates, potentially yielding nonvanishing rates even for molecules currently exhibiting zero. Given that the primary objective of our research is to illustrate the design of INVEST compounds rather than to predict rates with high precision, we acknowledge the limitations of our methodology. While our approach may not achieve the high degree of accuracy described in other works,[63,64] it remains a suitable and effective approach for our purposes. Incorporating the effects of vibrations in spin−orbit coupling and including nonadiabatic coupling can significantly enhance the accuracy of rate predictions. These factors have been emphasized in numerous critical studies,[65−67] which underscore their critical role in achieving more precise results.

4. CONCLUSIONS

In this study, we explored the photophysical properties of emitters tailored for OLED applications, employing an electronic structure framework as our guiding compass. Our primary objective was to engineer emitters with a triplet state (T_1) energy surpassing the singlet state (S_1). Leveraging computational methodologies such STEOM-DLPNO−CCSD, which adeptly accounts for double excitations in both singlet and triplet states, we successfully assessed the singlet−triplet energy gap (ΔE_{ST}) across a diverse array of emitters. Our investigation spanned a spectrum of 32 compounds, where a remarkable 72% success rate in identifying INVEST emitters underscored the efficacy of our approach. We streamlined the design process by employing straightforward molecular cores, yielding INVEST molecules with commendable oscillator strength values, peaking at 0.013.

Our analysis confined critical parameters like exchange integrals, HOMO−LUMO overlap, and dynamic spin-polarization (DSP) values, which are pivotal for ensuring a negative singlet−triplet gap. Noteworthy trends emerged, with pentalene-containing compounds consistently manifesting negative ΔE_{ST} values while their naphthalene counterparts exhibited contrasting behavior. This subtle understanding was supported by insights into exciton characteristics, unveiling a predominance of short-range charge transfer during the S_1 to S_0 transition. The design strategy was further validated through density difference plots and spin−orbit coupling assessments, elucidating well-separated energy levels and emphasizing the pivotal role of spin−orbit coupling in facilitating high rates of reverse intersystem crossing, reaching a remarkable 10^7 s^{-1}. Our study serves as a testament to the efficacy of such strategic approaches in engineering highly efficient emitters tailored for optoelectronic applications. By unraveling the intricate interplay of molecular structure and photophysical behavior, we pave the way for the next generation of advanced materials poised to redefine the landscape of OLED technology.

■ ASSOCIATED CONTENT

Supporting Information

The Supporting Information is available free of charge at https://pubs.acs.org/doi/10.1021/acs.jpca.4c03443.

Sample input file; the methodology to calculate the k_{PF} and k_{DF} rates; molecular structures; frontier molecular orbital picture of the investigated compounds, the density difference plots for the T_1 to S_1 transition, and tabulated values of excited state energies, coupling, and rates (PDF)

Opt coordinates (ZIP)

■ AUTHOR INFORMATION

Corresponding Author

Anirban Mondal − *Department of Chemistry, Indian Institute of Technology, Gandhinagar, Gujarat 382355, India;* orcid.org/0000-0003-3029-8840; Email: amondal@iitgn.ac.in

Authors

Sanyam − *Department of Chemistry, Indian Institute of Technology, Gandhinagar, Gujarat 382355, India;* orcid.org/0000-0001-7410-8207

Priyanshu Sorout − *Department of Chemistry, Indian Institute of Technology, Gandhinagar, Gujarat 382355, India*

Complete contact information is available at: https://pubs.acs.org/10.1021/acs.jpca.4c03443

Author Contributions

†S. and P.S. contributed equally to this work.

Notes

The authors declare no competing financial interest.

■ ACKNOWLEDGMENTS

The authors gratefully acknowledge the Indian Institute of Technology Gandhinagar, India, for providing the research facilities and support. A.M. acknowledges the SERB (SRG/2022/001532) project for funding. S. thanks CSIR for the fellowship. We thank PARAM Ananta for computational resources.

■ REFERENCES

(1) Endo, A.; Sato, K.; Yoshimura, K.; Kai, T.; Kawada, A.; Miyazaki, H.; Adachi, C. Efficient up-conversion of triplet excitons into a singlet state and its application for organic light emitting diodes. *Appl. Phys. Lett.* **2011**, *98*, No. 083302.

(2) Liu, Y.; Li, C.; Ren, Z.; Yan, S.; Bryce, M. R. All-organic thermally activated delayed fluorescence materials for organic light-emitting diodes. *Nat. Rev. Mater.* **2018**, *3*, No. 18020.

(3) Uoyama, H.; Goushi, K.; Shizu, K.; Nomura, H.; Adachi, C. Highly efficient organic light-emitting diodes from delayed fluorescence. *Nature* **2012**, *492*, 234−238.

(4) Shizu, K.; Kaji, H. Comprehensive understanding of multiple resonance thermally activated delayed fluorescence through quantum chemistry calculations. *Commun. Chem.* **2022**, *5*, No. 53.

(5) Kim, H. J.; Yasuda, T. Narrowband emissive thermally activated delayed fluorescence materials. *Adv. Opt. Mater.* **2022**, *10*, No. 2201714.

(6) Li, H.-Z.; Xie, F.-M.; Li, Y.-Q.; Tang, J.-X. Recent progress and prospects of fluorescent materials based on narrow emission. *J. Mater. Chem. C* **2023**, *11*, 6471−6511.

(7) Liu, S.; Langenaeker, W. Hund's multiplicity rule: a unified interpretation. *Theor. Chem. Acc.* **2003**, *110*, 338−344.

(8) Katriel, J.; Pauncz, R. Theoretical Interpretation of Hund's Rule. In *Advances in Quantum Chemistry*; Elsevier, 1977; Vol. *10*, pp 143−185.
(9) Sandoval-Salinas, M. E.; Ricci, G.; Pérez-Jiménez, A.; Casanova, D.; Olivier, Y.; Sancho-Garcia, J.-C. Correlation vs. exchange competition drives the singlet−triplet excited-state inversion in non-alternant hydrocarbons. *Phys. Chem. Chem. Phys.* **2023**, *25*, 26417−26428.
(10) Dubbini, M.; Bonvini, F.; Di Maiolo, F. Turning on Organic Radical Emitters *ChemRxiv* 2024 DOI: 10.26434/chemrxiv-2024-qghqc.
(11) Blasco, D.; Nasibullin, R. T.; Valiev, R. R.; Monge, M.; López-de Luzuriaga, J. M.; Sundholm, D. Experimental and computational studies of the optical properties of 2, 5, 8-tris (phenylthiolato) heptazine with an inverted singlet−triplet gap. *Phys. Chem. Chem. Phys.* **2024**, *26*, 5922−5931.
(12) Toyota, A.; Nakajima, T. Violation of Hund's multiplicity rule in the lowest excited singlet−triplet pairs of cyclic bicalicene and its higher homologues. *J. Chem. Soc., Perkin Trans. 2* **1986**, 1731−1734.
(13) Koseki, S.; Nakajima, T.; Toyota, A. Violation of Hund's multiplicity rule in the electronically excited states of conjugated hydrocarbons. *Can. J. Chem.* **1985**, *63*, 1572−1579.
(14) Pollice, R.; Friederich, P.; Lavigne, C.; dos Passos Gomes, G.; Aspuru-Guzik, A. Organic molecules with inverted gaps between first excited singlet and triplet states and appreciable fluorescence rates. *Matter* **2021**, *4*, 1654−1682.
(15) Leupin, W.; Wirz, J. Low-lying electronically excited states of cycl [3.3. 3] azine, a bridged 12. pi.-perimeter. *J. Am. Chem. Soc.* **1980**, *102*, 6068−6075.
(16) Li, J.; Nakagawa, T.; MacDonald, J.; Zhang, Q.; Nomura, H.; Miyazaki, H.; Adachi, C. Highly Efficient Organic Light-Emitting Diode Based on a Hidden Thermally Activated Delayed Fluorescence Channel in a Heptazine Derivative. *Adv. Mater.* **2013**, *25*, 3319−3323.
(17) Li, J.; Zhang, Q.; Nomura, H.; Miyazaki, H.; Adachi, C. Thermally activated delayed fluorescence from $3n\pi^*$ to $1n\pi^*$ up-conversion and its application to organic light-emitting diodes. *Appl. Phys. Lett.* **2014**, *105*, No. 013301, DOI: 10.1063/1.4887346.
(18) Li, J.; Nomura, H.; Miyazaki, H.; Adachi, C. Highly efficient exciplex organic light-emitting diodes incorporating a heptazine derivative as an electron acceptor. *Chem. Commun.* **2014**, *50*, 6174−6176.
(19) Ehrmaier, J.; Rabe, E. J.; Pristash, S. R.; Corp, K. L.; Schlenker, C. W.; Sobolewski, A. L.; Domcke, W. Singlet−triplet inversion in heptazine and in polymeric carbon nitrides. *J. Phys. Chem. A* **2019**, *123*, 8099−8108.
(20) Ricci, G.; San-Fabián, E.; Olivier, Y.; Sancho-García, J.-C. Singlet-triplet excited-state inversion in heptazine and related molecules: assessment of TD-DFT and ab initio methods. *ChemPhysChem* **2021**, *22*, 553−560.
(21) Aizawa, N.; Pu, Y.-J.; Harabuchi, Y.; Nihonyanagi, A.; Ibuka, R.; Inuzuka, H.; Dhara, B.; Koyama, Y.; Nakayama, K.-i.; Maeda, S.; et al. Delayed fluorescence from inverted singlet and triplet excited states. *Nature* **2022**, *609*, 502−506.
(22) de Silva, P. Inverted singlet−triplet gaps and their relevance to thermally activated delayed fluorescence. *J. Phys. Chem. Lett.* **2019**, *10*, 5674−5679.
(23) Bhattacharyya, K. Can TDDFT render the electronic excited states ordering of Azine derivative? A closer investigation with DLPNO-STEOM-CCSD. *Chem. Phys. Lett.* **2021**, *779*, No. 138827.
(24) Sanz-Rodrigo, J.; Ricci, G.; Olivier, Y.; Sancho-Garcia, J.-C. Negative singlet−triplet excitation energy gap in triangle-shaped molecular emitters for efficient triplet harvesting. *J. Phys. Chem. A* **2021**, *125*, 513−522.
(25) Dinkelbach, F.; Bracker, M.; Kleinschmidt, M.; Marian, C. M. Large inverted singlet−triplet energy gaps are not always favorable for triplet harvesting: Vibronic coupling drives the (reverse) intersystem crossing in heptazine derivatives. *J. Phys. Chem. A* **2021**, *125*, 10044−10051.
(26) Pu, Y.-J.; Valverde, D.; Sancho-García, J. C.; Olivier, Y. Computational Design of Multiple Resonance-Type BN Molecules for Inverted Singlet and Triplet Excited States. *J. Phys. Chem. A* **2023**, *127*, 10189−10196.
(27) Tučková, L.; Straka, M.; Valiev, R. R.; Sundholm, D. On the origin of the inverted singlet−triplet gap of the 5th generation light-emitting molecules. *Phys. Chem. Chem. Phys.* **2022**, *24*, 18713−18721.
(28) Garner, M. H.; Blaskovits, J. T.; Corminboeuf, C. Enhanced inverted singlet−triplet gaps in azaphenalenes and non-alternant hydrocarbons. *Chem. Commun.* **2024**, *60*, 2070−2073.
(29) Garner, M. H.; Blaskovits, J. T.; Corminboeuf, C. Double-bond delocalization in non-alternant hydrocarbons induces inverted singlet−triplet gaps. *Chem. Sci.* **2023**, *14*, 10458−10466.
(30) Omar, Ö. H.; Xie, X.; Troisi, A.; Padula, D. Identification of Unknown Inverted Singlet−Triplet Cores by High-Throughput Virtual Screening. *J. Am. Chem. Soc.* **2023**, *145*, 19790−19799.
(31) Ghosh, S.; Bhattacharyya, K. Origin of the failure of density functional theories in predicting inverted singlet−triplet gaps. *J. Phys. Chem. A* **2022**, *126*, 1378−1385.
(32) Pershin, A.; Hall, D.; Lemaur, V.; Sancho-Garcia, J.-C.; Muccioli, L.; Zysman-Colman, E.; Beljonne, D.; Olivier, Y. Highly emissive excitons with reduced exchange energy in thermally activated delayed fluorescent molecules. *Nat. Commun.* **2019**, *10*, No. 597.
(33) Sanyam; Khatua, R.; Mondal, A. Constructing Multiresonance Thermally Activated Delayed Fluorescence Emitters for Organic LEDs: A Computational Investigation. *J. Phys. Chem. A* **2023**, *127*, 10393−10405.
(34) Sanyam; Khatua, R.; Mondal, A. Cost-Effective Approach for Modeling of Multiresonant Thermally Activated Delayed Fluorescence Emitters. *J. Chem. Theory Comput.* **2023**, *19*, 9290−9301.
(35) Pariser, R.; Parr, R. G. A Semi-Empirical Theory of the Electronic Spectra and Electronic Structure of Complex Unsaturated Molecules. I. *J. Chem. Phys.* **1953**, *21*, 466−471.
(36) Pariser, R.; Parr, R. G. A semi-empirical theory of the electronic spectra and electronic structure of complex unsaturated molecules. II. *J. Chem. Phys.* **1953**, *21*, 767−776.
(37) Pariser, R. Theory of the electronic spectra and structure of the polyacenes and of alternant hydrocarbons. *J. Chem. Phys.* **1956**, *24*, 250−268.
(38) Pariser, R. Electronic spectrum and structure of azulene. *J. Chem. Phys.* **1956**, *25*, 1112−1116.
(39) Pople, J. A. Electron interaction in unsaturated hydrocarbons. *Trans. Faraday Soc.* **1953**, *49*, 1375−1385.
(40) Favini, G.; Vandoni, I.; Simonetta, M. Calculation of electronic spectra of aza-benzenes and aza-naphthalenes by the Pariser-Parr-Pople method. *Theor. Chim. Acta* **1965**, *3*, 45−58.
(41) Frisch, M. J.; Trucks, G. W.; Schlegel, H. B.; Scuseria, G. E.; Robb, M. A.; Cheeseman, J. R.; Scalmani, G.; Barone, V.; Mennucci, B.; Petersson, G. A.et al. *Gaussian 09*, Revision E.01; Gaussian Inc.: Wallingford CT, 2009.
(42) Kerru, N.; Gummidi, L.; Bhaskaruni, S. V.; Maddila, S. N.; Singh, P.; Jonnalagadda, S. B. A comparison between observed and DFT calculations on structure of 5-(4-chlorophenyl)-2-amino-1, 3, 4-thiadiazole. *Sci. Rep.* **2019**, *9*, No. 19280.
(43) Pratik, S. M.; Coropceanu, V.; Brédas, J.-L. Enhancement of thermally activated delayed fluorescence (TADF) in multi-resonant emitters via control of chalcogen atom embedding. *Chem. Mater.* **2022**, *34*, 8022−8030.
(44) Neese, F. The ORCA program system. *WIREs Comput. Mol. Sci.* **2012**, *2*, 73−78.
(45) Barone, V.; Cossi, M. Quantum calculation of molecular energies and energy gradients in solution by a conductor solvent model. *J. Phys. Chem. A* **1998**, *102*, 1995−2001.
(46) Lu, T.; Chen, F. Multiwfn: A multifunctional wavefunction analyzer. *J. Comput. Chem.* **2012**, *33*, 580−592.
(47) Li, J.; Li, Z.; Liu, H.; Gong, H.; Zhang, J.; Yao, Y.; Guo, Q. Organic molecules with inverted singlet-triplet gaps. *Front. Chem.* **2022**, *10*, No. 999856.

(48) Bedogni, M.; Giavazzi, D.; Di Maiolo, F.; Painelli, A. Shining Light on Inverted Singlet−Triplet Emitters. *J. Chem. Theory Comput.* **2024**, *20*, 902−913.
(49) Wang, J.; Hafeez, H.; Tang, S.; Matulaitis, T.; Edman, L.; Samuel, I. D.; Zysman-Colman, E. Highly efficient organic light-emitting diodes and light-emitting electrochemical cells employing multiresonant thermally activated delayed fluorescent emitters with bulky donor or acceptor peripheral groups. *Aggregate* **2024**, No. e571.
(50) Pollice, R.; Ding, B.; Aspuru-Guzik, A. Rational design of organic molecules with inverted gaps between the first excited singlet and triplet. *Matter* **2024**, *7*, 1161−1186.
(51) Blaskovits, J. T.; Garner, M. H.; Corminboeuf, C. Symmetry-Induced Singlet-Triplet Inversions in Non-Alternant Hydrocarbons. *Angew. Chem.* **2023**, *135*, No. e202218156.
(52) Heilbronner, E.; Yang, Z.-Z. The Influence of Substituents on Double-Bond Localization, eg in s-Indacene. *Angew. Chem., Int. Ed.* **1987**, *26*, 360−362.
(53) Kataoka, M.; Ohmae, T.; Nakajima, T. Effects of electron-donating substituents on the bond alternations in pentalene and heptalene. *J. Org. Chem.* **1986**, *51*, 358−362.
(54) Kollmar, H.; Staemmler, V. A theoretical study of the structure of cyclobutadiene. *J. Am. Chem. Soc.* **1977**, *99*, 3583−3587.
(55) Kollmar, H.; Staemmler, V. Violation of Hund's rule by spin polarization in molecules. *Theor. Chim. Acta* **1978**, *48*, 223−239.
(56) Toyota, A. Violation of Hund's rule in the lowest excited singlet-triplet pairs of dicyclohepta [cd, gh] pentalene and dicyclopenta [ef, kl] heptalene. *Theor. Chim. Acta* **1988**, *74*, 209−217.
(57) Jorner, K.; Pollice, R.; Lavigne, C.; Aspuru-Guzik, A. Ultrafast Computational Screening of Molecules with Inverted Singlet−Triplet Energy Gaps Using the Pariser−Parr−Pople Semiempirical Quantum Chemistry Method. *J. Phys. Chem. A* **2024**, *128*, 2445−2456.
(58) Hall, D.; Sancho-García, J. C.; Pershin, A.; Ricci, G.; Beljonne, D.; Zysman-Colman, E.; Olivier, Y. Modeling of multiresonant thermally activated delayed fluorescence emitters—properly accounting for electron correlation is key! *J. Chem. Theory Comput.* **2022**, *18*, 4903−4918.
(59) Xu, S.; Yang, Q.; Wan, Y.; Chen, R.; Wang, S.; Si, Y.; Yang, B.; Liu, D.; Zheng, C.; Huang, W. Predicting intersystem crossing efficiencies of organic molecules for efficient thermally activated delayed fluorescence. *J. Mater. Chem. C* **2019**, *7*, 9523−9530.
(60) Aizawa, N.; Harabuchi, Y.; Maeda, S.; Pu, Y.-J. Kinetic prediction of reverse intersystem crossing in organic donor−acceptor molecules. *Nat. Commun.* **2020**, *11*, No. 3909.
(61) Serdiuk, I. E.; Mońka, M.; Kozakiewicz, K.; Liberek, B.; Bojarski, P.; Park, S. Y. Vibrationally Assisted Direct Intersystem Crossing between the Same Charge-Transfer States for Thermally Activated Delayed Fluorescence: Analysis by Marcus−Hush Theory Including Reorganization Energy. *J. Phys. Chem. B* **2021**, *125*, 2696−2706.
(62) Fornari, R. P.; Aragó, J.; Troisi, A. A very general rate expression for charge hopping in semiconducting polymers. *J. Chem. Phys.* **2015**, *142*, No. 184105, DOI: 10.1063/1.4920945.
(63) de Sousa, L. E.; de Silva, P. Unified framework for photophysical rate calculations in tadf molecules. *J. Chem. Theory Comput.* **2021**, *17*, 5816−5824.
(64) Penfold, T. J.; Gindensperger, E.; Daniel, C.; Marian, C. M. Spin-vibronic mechanism for intersystem crossing. *Chem. Rev.* **2018**, *118*, 6975−7025.
(65) Chen, X.-K.; Zhang, S.-F.; Fan, J.-X.; Ren, A.-M. Nature of highly efficient thermally activated delayed fluorescence in organic light-emitting diode emitters: nonadiabatic effect between excited states. *J. Phys. Chem. C* **2015**, *119*, 9728−9733.
(66) Gibson, J.; Monkman, A. P.; Penfold, T. J. The importance of vibronic coupling for efficient reverse intersystem crossing in thermally activated delayed fluorescence molecules. *ChemPhysChem* **2016**, *17*, 2956−2961.
(67) Marian, C. M. Mechanism of the triplet-to-singlet upconversion in the assistant dopant ACRXTN. *J. Phys. Chem. C* **2016**, *120*, 3715−3721.

https://doi.org/10.1021/acs.jpca.4c03443
J. Phys. Chem. A XXXX, XXX, XXX−XXX